SURFACE CHEMISTRY

Chemical bond formation showing a transition from physisorption to chemisorption

Ferdinand Huber[1], Julian Berwanger[1], Svitlana Polesya[2], Sergiy Mankovsky[2], Hubert Ebert[2], Franz J. Giessibl[1]*

Surface molecules can transition from physisorption through weak van der Waals forces to a strongly bound chemisorption state by overcoming an energy barrier. We show that a carbon monoxide (CO) molecule adsorbed to the tip of an atomic force microscope enables a controlled observation of bond formation, including its potential transition from physisorption to chemisorption. During imaging of copper (Cu) and iron (Fe) adatoms on a Cu(111) surface, the CO was not chemically inert but transited through a physisorbed local energy minimum into a chemisorbed global minimum, and an energy barrier was seen for the Fe adatom. Density functional theory reveals that the transition occurs through a hybridization of the electronic states of the CO molecule mainly with s-, p_z-, and d_{z^2}-type states of the Fe and Cu adatoms, leading to chemical bonding.

The physicist Richard Feynman believed that the sentence "...all things are made of atoms—little particles that move around in perpetual motion, attracting each other when they are a little distance apart, but repelling upon being squeezed into one another" (*1*) contains the most information about scientific knowledge in the fewest words. Although this quote captures the key characteristics of chemical bonding, subtle complications do occur in nature. In 1932, Lennard-Jones described that molecules can bond to a surface in two ways [see figure 3 in (*2*)]: a weak bond induced by van der Waals (vdW) attraction (physisorption) and, for smaller distances, a stronger chemical bond (chemisorption). In some cases, these two bonding regimes are split by an energetic barrier and, depending on the height of the barrier, transitions can occur [see figure 9.5 in (*3*)]. Overall, three different bonding scenarios can evolve (*3*, *4*):

1) The formation of a weak physical bond (vdW bond) with depth of ≈20 meV (0.46 kcal/mol) as shown by the potential energy V versus distance z curve in Fig. 1A and its corresponding force curve $F_z(z)$ in Fig. 1D with a maximal attractive force (*5*) on the order of 10 pN. The interaction of two noble gas atoms such as Xe is an example of such an interaction.

2) The formation of a strong chemical bond with energies on the order of electron volts shown in Fig. 1B, where the attractive force (Fig. 1E) can reach nanonewtons and mask the ever-present vdW forces that are on the order of 10 pN, followed by repulsion at small z. The data in Fig. 1, B and E, correspond to the bonding energy and vertical force between two Si atoms according to the Stillinger-Weber potential (*6*).

3) The third bonding mechanism involves a transition from physisorption to chemisorption as shown in Fig. 1C (*3*, *4*). The initial appearance of a weak vdW bond is followed by a transition that can show an energy barrier of high strength (black curve in Fig. 1C), a medium barrier (green and red curves), and a vanishing barrier (blue curve). If a molecule arrives at the surface with sufficient thermal energy to overcome the slight energy barrier of the green energy curve in Fig. 1C, it can chemisorb immediately. If a stronger energy barrier occurs, as shown by the black curve in Fig. 1C, its energy needs to be lifted by thermal excitation to overcome the barrier and to form a strong chemical bond (Fig. 1F). The $V(z)$ curve in Fig. 1C is key to the physisorption-chemisorption transition and possible subsequent heterogeneous catalysis. Whereas previous methods only provided the equilibrium positions at their corresponding temperatures, state-of-the-art atomic force microscopy (AFM) at low temperatures can directly record this curve.

Carbon monoxide can undergo physisorption as well as molecular and dissociative chemisorption on transition metal surfaces. Dissociative chemisorption to adsorbed C and O atoms tends to prevail on all transition metals in the periodic table left of a boundary between iron and cobalt at room temperature [chapter 6.4.1 in (*4*), and (*7*, *8*)], as well as for W (*9*). Conventional methods for adsorption studies, such as thermal desorption spectroscopy or electron energy loss spectroscopy (*3*, *4*), probe large molecular ensembles. Chemisorption is key to heterogeneous catalysis, and detailed knowledge about its basic mechanism can be obtained by using scanning tunneling microscopy (STM) as an atomic probe (*10*). Although STM combined with ultrashort laser pulsing has recently obtained femtosecond time resolution in imaging the surface vibrations of molecules (*11*), STM has thus far been used to image the end products of surface reactions and not the reactions themselves.

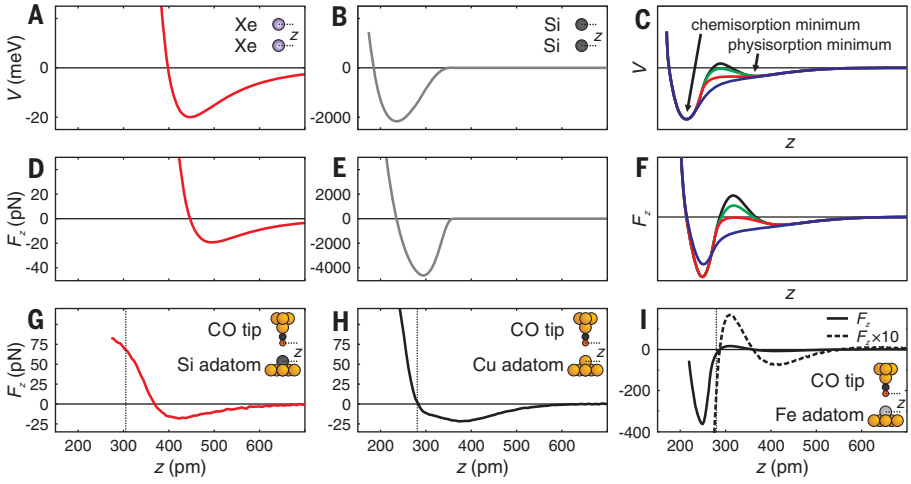

Fig. 1. Force and energy versus distance curves for various bonding situations. (**A** to **C**) Schematic potential energy V and (**D** to **F**) vertical force F_z versus distance z curves for [(A) and (D)] a weak physical bond, [(B) and (E)] a strong chemical bond, and [(C) and (F)] a bond with a transition from physisorption to chemisorption. The colored curves in (C) and (F) show four different cases that vary by their barrier height. If a repulsive energy barrier exists (i.e., $V > 0$ in the region between physisorption and chemisorption as shown with a black curve), the adsorbate may just reach the physisorbed state. For a very low energy barrier (green curve), thermal excitation can suffice to bring the adsorbate into a chemisorbed state, and for the red and blue curves, the adsorbate will immediately end up in the chemisorbed state. (**G** to **I**) Experimental force versus distance curves showing various bonds between the CO-terminated tip and (G) a Si adatom (*24*), (H) a Cu adatom, and (I) a Fe adatom on Cu(111). The potential energy curve corresponding to (I) is shown in fig. S10.

[1]Institute of Experimental and Applied Physics, Department of Physics, University of Regensburg, 93040 Regensburg, Germany. [2]Department of Chemistry, Ludwig-Maximilians-Universität München, 81377 Munich, Germany.
*Corresponding author. Email: franz.giessibl@ur.de

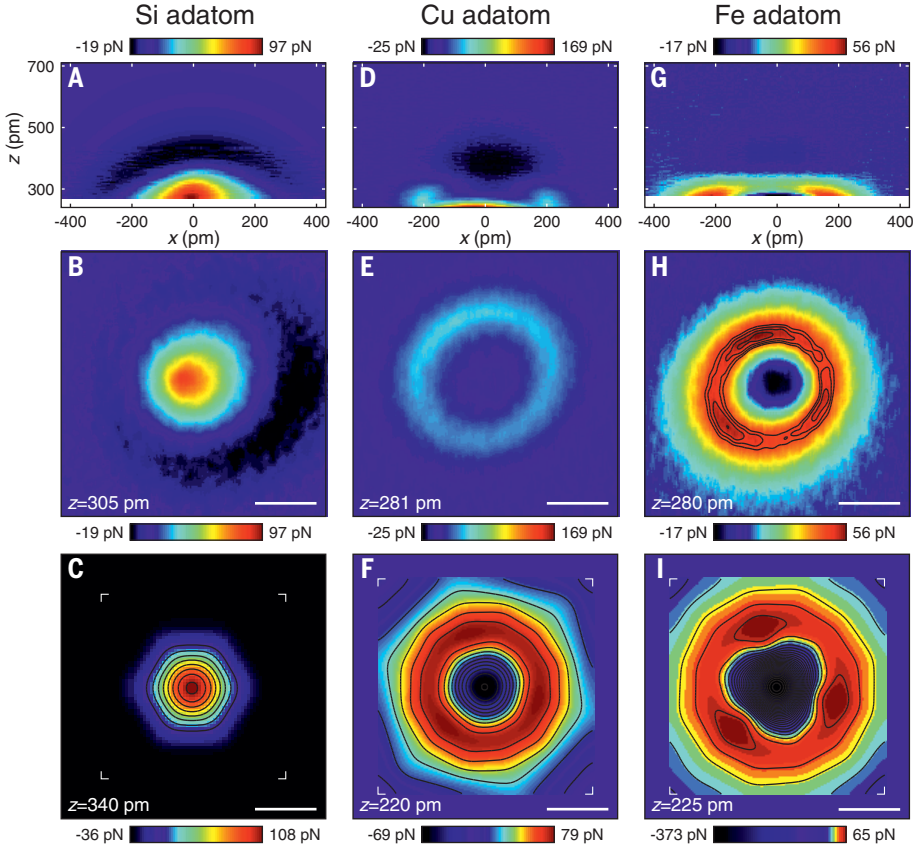

Fig. 2. Experimental and calculated forces for three different adatoms in side and top views. Top row (side view): Experimental vertical forces F_z in the *xz* plane between a CO-terminated AFM tip and (**A**) a Si adatom, (**D**) a Cu adatom, and (**G**) a Fe adatom on Cu(111). Middle row (top view): Constant-height force data in the *xy* plane between a CO-terminated tip and (**B**) a Si adatom, (**E**) a Cu adatom, and (**H**) a Fe adatom on Cu(111) taken at *z* positions, as indicated by vertical dotted lines in Fig. 1, G to I, respectively. Bottom row (top view): DFT calculations of F_z in the *xy* plane between a CO molecule tip and (**C**) a Si adatom, (**F**) a Cu adatom, and (**I**) a Fe adatom on Cu(111). The three local maxima on the experimental data (H) and DFT data (I) for the Fe adatom are located above the hollow sites of the Cu(111) substrate underneath (see figs. S5 and S6). Note that the color scale is the same for the force data in the top and middle rows. The color scale in the bottom row is different in order to maximize the contrast. Scale bars, 200 pm.

AFM (*12*) and its variants (*13*, *14*) have become a powerful tool for surface studies (*15*). The attachment of a CO molecule to an STM tip can enhance resolution by creating a sharper probe tip (*16*), and Gross *et al.* reported that CO-terminated AFM tips allow imaging of organic molecules with intramolecular resolution (*17*), leading to wide use of CO-terminated tips (*18*). The inertness of CO-terminated tips enabled imaging of many organic molecules (*18*) and graphene (*19*), as well as metal clusters and the silicon (111)-(7×7) surface (*20*), at unprecedented resolution. The use of CO-terminated AFM tips allows the tracking of the formation and potential transition from physisorption to chemisorption of a bond as a function of distance (i.e., reaction coordinate) for a single CO molecule with a precisely controlled position on a picometer scale.

There is a restriction imposed by the bond of the CO molecule to the tip. A CO molecule in the gas phase can orient itself freely on a surface to enable the maximal bonding strength. In metal carbonyls such as $Ni(CO)_4$ or $Fe(CO)_5$, CO bonds with the C atom to the transition metal (*21*) and CO bonds to the AFM's metal tip in a similar manner. Experimental and theoretical evidence holds that the oxygen end of the CO-terminated tip is chemically inert. When imaging pentacene with CO-terminated tips (*17*), density functional theory (DFT) has shown that Pauli repulsion between electrons provides the contrast (*22*, *23*).

The bottom row in Fig. 1 displays experimental $F_z(z)$ curves over the centers of three different adatoms obtained with CO-terminated tips. Figure 1G shows the interaction of a CO-terminated tip with a single Si adatom on Cu(111), as indicated in the inset. The attractive vdW force reached only −20 pN before Pauli repulsion forces dominated (*24*). The interaction of the CO-terminated tip with the Si adatom resembled physisorption—a weak attraction turns to Pauli repulsion with a single energetic minimum. The strong covalent bonds with a magnitude of nanonewtons shown in Fig. 1, B and E, were used to atomically resolve AFM images in vacuum on the silicon surface (*25*), where DFT identified a covalent character (*26*) that was verified by precise force spectroscopy (*27*, *28*).

Figure 1H shows the $F_z(z)$ curve for a CO-terminated tip over a Cu adatom on Cu(111). The attractive force minimum was at z = 373 pm, and the attractive z range was widened compared with the Si curve in Fig. 1G. Figure 1I shows the $F_z(z)$ curve for a CO-terminated tip over a Fe adatom on Cu(111), which resembles the qualitative physisorption-chemisorption transition of Fig. 1F (black curve). The physisorbed force minimum of −8 pN at z = 420 pm was followed by a force barrier of +17 pN at z = 310 pm and a maximal attractive force of −364 pN at z = 250 pm. The occurrence of a barrier in the experimental force curve for the Fe adatom in Fig. 1I and its similarity to the schematic force curves pertaining to a physisorption-chemisorption transition in Fig. 1F pointed to the experimental observation of such a transition, as elucidated below.

The $F_z(z)$ curves in Fig. 1, G to I, were measured with the CO-terminated tip exactly centered over the adatoms. However, F is not merely a function of absolute distance between the centers of the O atom of the tip and the adatom, it is also a function of the polar and azimuthal angles with respect to the surface normal and substrate orientation. The top row of Fig. 2 shows F in the z direction as a function of lateral x direction and z position at y = 0. The force fields for the three different adatoms were distinctly different in the *xz* plane. The force curves in Fig. 1, G to I, are traces of the two-dimensional force fields $F_z(x, y, z)$ at $x = y = 0$. The middle row shows experimental constant-height force images of the three adatoms. The bottom row displays DFT force calculations for the three different adatoms.

The left column of Fig. 2 shows data for the simplest case, the Si adatom. For the force data of the Si adatom on the *xz* plane in Fig. 2A, we initially found weak vdW attraction followed by strong Pauli repulsion that was roughly proportional to the total charge density of the Si adatom as displayed in fig. S1A. The Si adatom appeared in the *xy* plane (Fig. 2B) as a Gaussian-shaped repulsion, showing that the CO-terminated tip interacted with it in a similar manner as it does with organic molecules.

Simulations of this image for four different heights using the probe particle model (*29*, *30*) are shown in fig. S2, where the lateral bending of the CO-terminated tip (*31*) was taken into account. The DFT calculation of the force image (Fig. 2C) yielded a result similar to that of

the experimental data (*32*). Because Pauli repulsion was the contrast mechanism here, the experimental images resembled the total charge densities presented in fig. S1A. DFT confirmed that Pauli repulsion was the contrast mechanism—differential charge density plots and calculations of the energies of the states (see figs. S7, A to D, and S8, A to F) showed no evidence for chemical bonding.

For the Cu adatom data (middle column of Fig. 2), in the center at $x \approx 0$ in Fig. 2D, vdW attraction was followed by some more slight attraction before turning to Pauli repulsion. The circumference of the Cu adatom at $x \approx \pm 200$ pm looked completely different with a transition from vdW attraction directly to Pauli repulsion. Accordingly, the constant-height data in Fig. 2E shows a ringlike appearance. The DFT calculation in Fig. 2F resembles the experimental data in Fig. 2E and is vastly different from the total charge density of the Cu adatom shown in fig. S1B. The evolution of the contrast with distance starts from the attractive vdW signature, changes to the repulsive ring, and ends in a repulsive cusp in the center, as shown in detail in fig. S3. The calculated $F_z(z)$ curves (fig. S7E), differential charge density plots (fig. S7, F to H), and pronounced shifts in the energies of the electronic states (fig. S8, G to M) provided a consistent dataset indicating the emergence of a medium-strength bond (*33*). The physical origin for the delayed transition from vdW attraction to Pauli repulsion is a hybridization of the electronic states of the Cu adatom with the states of the CO-terminated tip (*34*).

For the Fe adatom (right column of Fig. 2), in the center at $x \approx 0$ in Fig. 2G, the interaction started with vdW attraction (dark lenticular area at $z \approx 400$ pm), followed by weak repulsion (light-green lenticular area at $z \approx 330$ pm). After penetrating the repulsive barrier in the center, attraction occurred (see also Fig. 1I). For even smaller z, we expected repulsion again, but this close distance is not accessible because approaching to such close distances risked the integrity of the CO-terminated tip (*35*). Outside the center, at $x \approx \pm 210$ pm, we saw a direct transition from vdW attraction to Pauli repulsion similar to the circumference of the Cu adatom. The top view at Fig. 2H shows a repulsive ring similar to the Cu adatom, but for the Fe adatom, three local maxima were located over the hollow sites of the underlying Cu(111) surface (see figs. S5 and S6). The DFT force calculations presented in Fig. 2I confirmed the presence of three local maxima on the repulsive ring in registry with the Cu(111) substrate (see fig. S6).

As in the case of the Cu adatom, the images of the Fe adatom did not relate to the total charge density of the Fe adatom shown in fig. S1C. The physical origin of the ringlike appearance and strong attraction in the center of the Fe adatom was a hybridization of electronic states between tip and sample as revealed by the DFT calculations. The $F_z(z)$ curves (fig. S7I), differential charge density plots (fig. S7, J to L), and pronounced shifts in the energies of the electronic states of the CO-terminated tip and Fe adatom (fig. S8, N to T) provided a coherent picture of the formation of a chemical bond resulting from hybridization (*33*). We note that the appearance of the Cu and Fe adatoms as repulsive tori is not an artifact of bending of the CO-terminated tip (*31*) (see fig. S9).

The experimental images of Cu and Fe adatoms showed similarities and differences. Both appear as repulsive tori when imaged with CO-terminated tips at close distance. However, the Fe adatom showed three distinctive local maxima on the torus, and the attractive force in the center reached values down to −364 pN, whereas the center of the Cu adatom was much less attractive and even allowed to image the repulsive cusp for very small distances. Previous experiments have shown that single Fe adatoms on Cu(111) have a magnetic moment (*36*). Our DFT calculations confirm this and find zero magnetic moment for the Cu adatom. Thus, the physical origin of the difference in the AFM data of Cu versus Fe adatoms is the element-specific occupation of the majority and minority 3d spin states (see fig. S12).

We have shown that CO-terminated tips can hybridize with sample atoms and produce a contrast that is much different from the total charge density. The subatomic contrast (*20*), i.e., the appearance of nontrivial structures within images of single atoms, was explained as a signature of hybridization of states with a s, p, and d character in the formation of chemical bonds. The present findings extend atomically resolved force microscopy into a previously unexplored interaction regime. When atomically resolved AFM in vacuum was introduced 25 years ago, strong covalent or ionic bonds were probed in a noncontact distance regime, and noncontact AFM and atomically resolved AFM have, historically, often been considered synonymous. The introduction of CO-terminated tips by Gross *et al.* (*17*), as well as noble gas and other inert tips (*37*), expanded the distance regime where nondestructive atomically resolved images are possible from the noncontact regime to an intermittent-contact mode that probes Pauli repulsion forces.

The present work further expands AFM into a distance regime where the hybridizations occur that underlie the chemical bond. Possible applications include the study of partially unfilled Cu 3d states in cuprate superconductors (*38*). We showed that CO-terminated tips are not generally chemically inert, as tips terminated by noble gas atoms are. Therefore, CO-terminated tips do not generally interact via Pauli repulsion with the total charge density of the sample. This might change the interpretation of images of organic molecules that contain metal ions, in particular those with unfilled 3d shells.

REFERENCES AND NOTES

1. R. P. Feynman, R. B. Leighton, M. Sands, *The Feynman Lectures on Physics I* (Addison-Wesley, 1963), chaps. 1–2.
2. J. E. Lennard-Jones, *Trans. Faraday Soc.* **28**, 333–359 (1932).
3. A. Zangwill, *Physics at Surfaces* (Cambridge Univ. Press, 1988).
4. H. Ibach, *Physics of Surfaces and Interfaces* (Springer, 2006).
5. The potential energy V of a bond as a function of distance z between the atoms has its minimum at the bonding distance $z = \sigma$. Here, we display the force F_z that is given by the negative derivative of the potential energy with respect to distance with $F_z = -\partial V/\partial z$ with $F_z(\sigma) = 0$. The shapes of the $F_z(z)$ and $V(z)$ curves are very similar except for a lateral shift—$V(\sigma)$ is the minimal energy with $F_z(\sigma) = 0$. This similarity of overall shape and lateral shift also holds for more complex potentials that involve a repulsive barrier.
6. F. H. Stillinger, T. A. Weber, *Phys. Rev. B* **31**, 5262–5271 (1985).
7. G. Brodén, T. N. Rhodin, C. Brucker, R. Benbow, Z. Hurych, *Surf. Sci.* **59**, 593–611 (1976).
8. S.-S. Sung, R. Hoffmann, *J. Am. Chem. Soc.* **107**, 578–584 (1985).
9. F. M. Propst, T. C. Piper, *J. Vac. Sci. Technol.* **4**, 53–56 (1967).
10. G. Ertl, *Angew. Chem. Int. Ed.* **47**, 3524–3535 (2008).
11. T. L. Cocker, D. Peller, P. Yu, J. Repp, R. Huber, *Nature* **539**, 263–267 (2016).
12. G. Binnig, C. F. Quate, C. Gerber, *Phys. Rev. Lett.* **56**, 930–933 (1986).
13. T. R. Albrecht, P. Grütter, D. Horne, D. Rugar, *J. Appl. Phys.* **69**, 668–673 (1991).
14. U. Dürig, O. Züger, A. Stalder, *J. Appl. Phys.* **72**, 1778–1798 (1992).
15. R. García, R. Pérez, *Surf. Sci. Rep.* **47**, 197–301 (2002).
16. L. Bartels, G. Meyer, K.-H. Rieder, *Appl. Phys. Lett.* **71**, 213–215 (1997).
17. L. Gross, F. Mohn, N. Moll, P. Liljeroth, G. Meyer, *Science* **325**, 1110–1114 (2009).
18. N. Pavliček, L. Gross, *Nat. Rev. Chem.* **1**, 0005 (2017).
19. M. P. Boneschanscher *et al.*, *ACS Nano* **6**, 10216–10221 (2012).
20. M. Emmrich *et al.*, *Science* **348**, 308–311 (2015).
21. L. Pauling, *The Nature of the Chemical Bond* (Cornell Univ. Press, ed. 3, 1960).
22. N. Moll, L. Gross, F. Mohn, A. Curioni, G. Meyer, *New J. Phys.* **12**, 125020 (2010).
23. N. Moll, L. Gross, F. Mohn, A. Curioni, G. Meyer, *New J. Phys.* **14**, 083023 (2012).
24. CO bending (*31*) is responsible for the experimental observation of a decreasing slope of the force curve in Fig. 1G for close distances.
25. F. J. Giessibl, *Science* **267**, 68–71 (1995).
26. R. Pérez, M. C. Payne, I. Štich, K. Terakura, *Phys. Rev. Lett.* **78**, 678–681 (1997).
27. M. A. Lantz *et al.*, *Science* **291**, 2580–2583 (2001).
28. Y. Sugimoto *et al.*, *Nature* **446**, 64–67 (2007).
29. P. Hapala *et al.*, *Phys. Rev. B* **90**, 085421 (2014).
30. P. Hapala, R. Temirov, F. S. Tautz, P. Jelínek, *Phys. Rev. Lett.* **113**, 226101 (2014).
31. L. Gross *et al.*, *Science* **337**, 1326–1329 (2012).
32. The apparent 6-fold symmetry in the DFT data is an artifact originating from a relatively low number of calculated data points.
33. R. Hoffmann, *Rev. Mod. Phys.* **60**, 601–628 (1988).
34. In a previous publication (*20*), we provided a hypothesis to explain the ringlike structure of Cu and Fe adatoms that was compatible with the interpretation of CO-terminated tips imaging the total charge density of the sample, similar to what was found by Moll *et al.* (*22, 23*) for organic molecules. The ringlike structure of Fe and Cu adatoms was explained by a sp-hybridization of the adatom's 4s electrons to a $4sp_z$ orbital that displays a torus-shaped total charge density when observed from above. However, the DFT calculations shown in figs. S1, S7,

and S8, as well as the experimental observation of the repulsive barrier above the Fe adatom, showed that the hybridization occurs only under the presence of the CO-terminated tip and it involves not only s and p states but also d states.
35. The CO-terminated tip can come quite close to the Fe adatom when located at the center of the Fe adatom where lateral forces are zero. In Fig. 1I, the tip was even approached almost to the equilibrium distance where the force is zero again after passing the maximal attraction of −364 pN at the distance of 250 pm. The minimal distance that can be sustained by the AFM tip without losing its CO termination is determined by experience. Usually, tip loss is imminent when the driving signal that controls the constant oscillation amplitude of the force sensor starts to rise, i.e., when damping of the sensor owing to the tip-sample interaction becomes noticeable. When scanning in the *xy* plane, lateral forces act on the CO-terminated tip and larger distances are required to prevent the loss of the CO termination (compare Fig. 2G where the minimal distance was almost 100 pm larger than in the force spectrum of Fig. 1I).
36. G. E. Pacchioni *et al*., *Phys. Rev. B* **91**, 235426 (2015).
37. F. Mohn, B. Schuler, L. Gross, G. Meyer, *Appl. Phys. Lett.* **102**, 073109 (2013).
38. J. G. Bednorz, K. A. Müller, *Angew. Chem. Int. Ed.* **27**, 735–748 (1988).

ACKNOWLEDGMENTS

We thank J. Repp and A. J. Weymouth for discussions, G. Ertl and R. Hoffmann for helpful comments, and F. Stilp for support in data acquisition. **Funding:** We thank the Deutsche Forschungsgemeinschaft for funding under research project CRC1277, project A02. **Author contributions:** F.H. recorded parts of the experimental data, performed most of the data analysis, and visualized most of the data. J.B. recorded parts of and validated the experimental data. S.P. and S.M. conducted all DFT calculations, analyzed the DFT results, and visualized them. H.E. and F.J.G. are responsible for conceptualization, supervision of the project, and funding acquisition. F.J.G. prepared fig. S5 and wrote the manuscript (original draft). All authors reviewed and edited the manuscript. **Competing interests:** F.J.G. holds patents for the force sensor that was used in the experiment. All other authors declare no competing interests. **Data and materials availability:** All relevant data are available in the main text or the supplementary materials. All raw data and scripts that were used for the data analysis are stored in the computer center of the University of Regensburg and are available on request.

SUPPLEMENTARY MATERIALS

10 June 2019; accepted 29 August 2019
Published online 12 September 2019
10.1126/science.aay3444

Chemical bond formation showing a transition from physisorption to chemisorption

Ferdinand Huber, Julian Berwanger, Svitlana Polesya, Sergiy Mankovsky, Hubert Ebert and Franz J. Giessibl

Science **366** (6462), 235-238.
DOI: 10.1126/science.aay3444originally published online September 12, 2019

Imaging a chemisorption process

At low temperatures, a molecule may adsorb to a surface only through weak forces (physisorption), and only upon heating and overcoming an energetic barrier does it form a strong covalent bond (chemisorption). Huber *et al.* imaged this transition for an atomic force microscopy tip terminating in a carbon monoxide molecule. Although the oxygen atom of the tip is normally considered to act like a rare gas atom, interacting only through van der Waals interactions, at short distances directly above a transition metal atom, it transitions to a strongly interacting chemisorption state.

Science, this issue p. 235